

Stimulated Electromagnetic Emission: A New Technique to Study the Parametric Decay Instability in the Ionosphere

P. STUBBE AND H. KOPKA

Max-Planck-Institut für Aeronomie, Katlenburg-Lindau, Federal Republic of Germany

B. THIDÉ AND H. DERBLÖM

Uppsala Ionospheric Observatory, Sweden

A powerful HF wave, transmitted in the *O* mode with a frequency not exceeding the critical *F* region frequency, gives rise to secondary electromagnetic radiation, filling a frequency band of several 10 kHz around the frequency of the primary wave. The spectrum of these secondary waves is richly structured. The systematically occurring spectral features are identified and described. The majority of these features can be understood by scatter processes involving Langmuir waves and low-frequency density perturbations excited by the parametric decay instability. Other features, including a broad spectral maximum at 20 to 40 kHz on the upshifted side, are not as yet fully understood.

1. INTRODUCTION

Measurements of the spectrum of a strong ionospherically reflected electromagnetic wave, generated by the Heating facility at Ramfjordmoen near Tromsø, Norway [Stubbe *et al.*, 1982], showed that secondary electromagnetic waves are generated within the ionosphere [Thidé *et al.*, 1981, 1983]. These secondary waves exist within a frequency range of several 10 kHz around the frequency of the primary wave. Mostly, the downshifted portion of the spectrum is much more pronounced than the upshifted, but the converse is also possible. We term the phenomenon of secondary electromagnetic wave generation "stimulated electromagnetic emission."

Up to date we have collected a few thousand such spectra, and we are now able to define the regular and the occasional features. Experimental results are presented in sections 2 and 6. The data shown in section 2 are those that can be interpreted by means of the processes discussed in section 3, whereas the data shown in section 6 are not yet fully understood.

The fact that the downshifted portion of the spectrum usually contains more energy than the upshifted had led us to the conjecture that the secondary electromagnetic radiation is caused by mode conversion of Langmuir waves that are produced by the parametric decay of the primary electromagnetic wave [Thidé *et al.*, 1983]. It is the objective of the present paper to pursue this idea to the extent that the individual spectral features can be linked to well-defined physical processes. No attempt will be made to quantitatively model the spectral intensities, and so an unmagnetized plasma will be assumed for the sake of simplicity.

A discussion of the relevant physical processes is given in section 3, and in section 4 the results of this discussion are applied to the experimental findings presented in section 2. In section 5 we discuss the similarities and differences between the stimulated emission and incoherent scatter techniques. We shall see that these two techniques ideally supplement each other.

2. EXPERIMENTAL RESULTS (FIRST PART)

The experimental equipment consisted of a HP 3585A spectrum analyzer, connected either to a short crossed dipole or a long crossed Balsley type antenna, optimized for reception at 5.423 MHz (which is one of our licensed frequencies). The latter had a gain approximately 15 dB higher than the first. The observations were made either at Lavangsdalen, 17 km south of the Heating facility, or at Seljelvnes, 40 km south of the Heating facility. The experimental results shown below all relate to transmission and reception in the *O* mode.

We see from Figures 1-4 that the following spectral features can be identified: (1) A broad asymmetric continuum around the carrier, (2) a pronounced maximum at approximately 10 kHz below the carrier (DM, for downshifted maximum), (3) a corresponding maximum at approximately 10 kHz above the carrier (UM, for upshifted maximum), (4) maxima at about 2 or 3 times the offset frequency of the downshifted maximum (2DM, 3DM), (5) maxima at about $\frac{1}{2}$ times the offset frequencies of the downshifted or upshifted maximum ($\frac{1}{2}$ DM, $\frac{1}{2}$ UM), and (6) peaks at 2-3 kHz below or above the carrier (DP, UP, for downshifted or upshifted peak, respectively).

1. Continuum: Figure 1 shows four examples of the continuum. Usually the continuum is highly asymmetric, with more energy on the downshifted side. The frequency range covered by the continuum is strongly variable, as can be seen by comparing the four spectra shown in Figure 1. The continuum is the only spectral feature that is always present when stimulated emission occurs, and thus the continuum is also seen in Figures 2-4. Occasionally the continuum is almost symmetrical around the carrier. An example of this is seen in Figure 4d. Only when the stimulated emission is weak is the continuum the sole spectral feature. When its strength grows, other spectral features show up, particularly the downshifted maximum.

2. Downshifted maximum (DM): A typical example of the DM is shown in Figure 2. Usually, the DM is asymmetric in the sense demonstrated by Figure 2b. A typical elevation out of the continuum is about 10 dB. The clearest ever obtained DM (and likewise 2DM and 3DM) is shown in Figure 3d. Other examples for the DM are seen in Figures 3a-3c, Figures

Copyright 1984 by the American Geophysical Union.

Paper number 4A0657.
0148-0227/84/004A-0657\$05.00

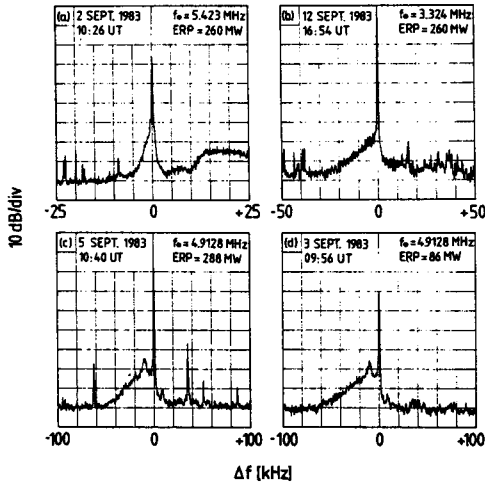


Fig. 1. Spectra to demonstrate the continuum. The date, heater frequency (f_0) and effective radiated power (ERP) are specified on the top of the individual spectra. The primary heating wave appears at $\Delta f = 0$. The other sharp spikes, for example, at -63 kHz and $+35$ kHz in spectrum (c), are due to interfering short wave stations. Both transmission and reception was in the mode.

4a and 4c, and Figures 9a–9c. The offset frequency of the DM, Δf_{DM} , shows a distinct dependence on the heating frequency f_0 , as illustrated by Figure 5. Usually, the stimulated emission is rather weak for heating frequencies above 6 and below 4 MHz. It is therefore not easy to obtain the dependence of the spectral features on the heating frequency. So far we have been successful only with respect to the DM, but there are indications that the 2DM, 3DM, $\frac{1}{2}$ DM, UM, and $\frac{1}{2}$ UM features possess corresponding dependencies on f_0 .

3. Upshifted maximum (UM): The UM is considerably weaker than the DM, by approximately 10 to 20 dB. Examples of the UM are shown by Figure 2a, Figures 3a–3d, Figures 4a, 4c, and 4d, and Figures 9a and 9c. Sometimes, the UM occurs at the mirror frequency of the DM (e.g., Figures 3b, 4a, and 4c), but more typically it peaks at a frequency offset that is up to 35% below the DM mirror frequency (e.g., Figures 3a and 2a). Sometimes, both these peaks occur simultaneously (e.g., Figure 3c), and so it appears that two different physical processes are needed to understand the UM.

4. 2DM, 3DM: The 2DM is seen in Figures 3a, 3b, and 3d and Figure 4a. The strength of the 2DM is approximately equal to that of the UM, but there are also cases (e.g., Figure 3d) where the two do not seem to be well correlated. The 3DM, shown by Figure 3d, is a very rare feature, and we have only a few examples that clearly prove its existence.

5. $\frac{1}{2}$ DM, $\frac{1}{2}$ UM: Both these features are rarely seen, the

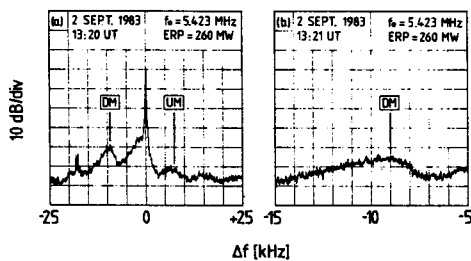


Fig. 2. Spectra to demonstrate the DM feature. Also seen is the UM feature. Further text as in Figure 1.

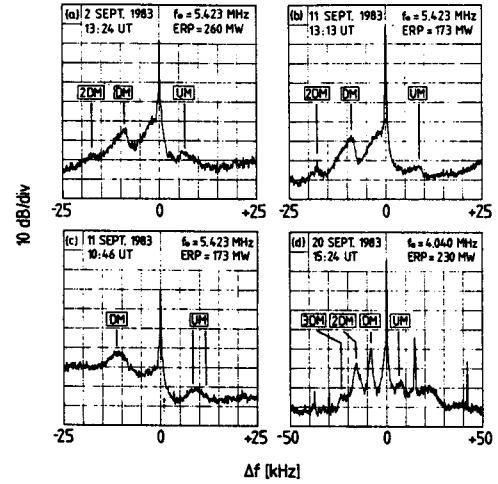


Fig. 3. Spectra to demonstrate the UM, 2DM, and 3DM features. Also seen are the DM and UM features. Further text as in Figure 1.

$\frac{1}{2}$ UM because it is weak, the $\frac{1}{2}$ DM because it usually appears to be masked by the continuum. Examples of the $\frac{1}{2}$ DM and $\frac{1}{2}$ UM are shown in Figures 4a–4d. Figure 4d depicts a rather unusual situation because it shows the $\frac{1}{2}$ DM and $\frac{1}{2}$ UM features while the DM is absent.

6. Downshifted and upshifted peak (DP, UP): The majority of our experiments were performed with one of the heating frequencies $f_0 = 4.04$, 4.9128, or 5.423 MHz. Curiously, the DP and UP have only been observed with $f_0 = 4.04$ MHz, although, when they appear, they are well developed and easy to identify. Examples are shown in Figures 4a and 4b. The DP is approximately 10 dB stronger than the UP.

The strongest spectra are obtained during periods of low magnetic activity, weak *D* region absorption, and well developed *F* region, as indicated by clear ionogram traces. During such optimum periods, a small fraction of the full available power (effective radiated power as low as 15 MW) is sufficient to cause stimulated electromagnetic emission, whereas at unfavorable times even full power (effective radiated power as high as 300 MW) does not produce measurable effects. It can therefore be ruled out that auroral conditions are needed in any way to produce stimulated emission.

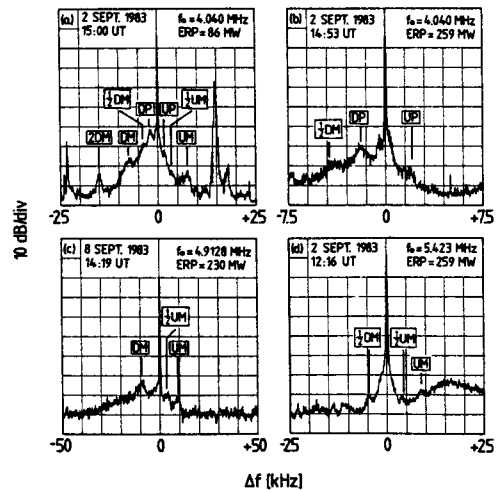


Fig. 4. Spectra to demonstrate the $\frac{1}{2}$ DM, $\frac{1}{2}$ UM, DP, and UP features. Also seen are the DM, UM and 2DM features. Further text as in Figure 1.

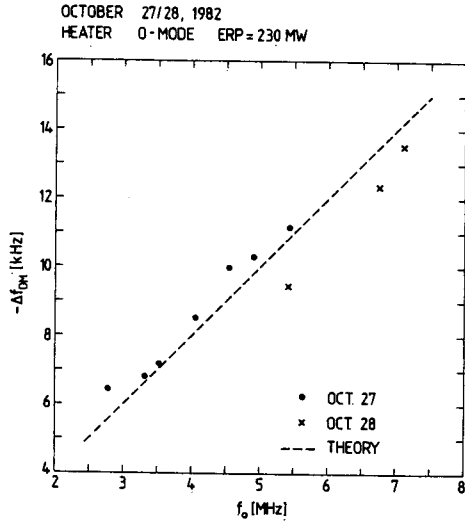


Fig. 5. Offset frequency of the DM, Δf_{DM} , as a function of heating frequency, f_0 . The dots and crosses are experimental values. The broken line is a theoretical curve, based on (31d).

3. THEORY

3.1. Assumptions and Nomenclature

The electron density in the vicinity of the reflection altitude, z_0 , of an O mode heating wave is described by a linear profile, i.e.,

$$\omega_p^2 = \omega_0^2(1 - 2\delta) \quad \delta \equiv \frac{z_0 - z}{2H} \quad (1a)$$

Here, ω_p is the local plasma frequency, ω_0 is the frequency of the O mode heating wave, and H is the linear electron density scale height. For small δ ,

$$\omega_p = \omega_0(1 - \delta) \quad (1b)$$

The waves present in the plasma are denoted in the following way: electromagnetic heating wave (EM), Langmuir waves generated by the parametric decay instability (LWD), Langmuir waves caused by cascading (LWC), i.e., by successive decay of Langmuir waves through the decay instability, Langmuir waves generated by the purely growing mode of the decay instability (LWG), ion acoustic waves generated by the decay instability (IAD), ion acoustic waves generated by the cascading process (IAC), and ion acoustic waves generated by the purely growing mode of decay instability (IAG). The latter are nonpropagating, purely spatial plasma density perturbations.

Alternatively, we denote these waves by their frequency-wave vector couples:

EM: (ω_0, \mathbf{k}_0)

$$\omega_0 = \text{heating frequency} \quad k_0 \approx 0 \quad (2a)$$

LWD: $(\omega_{1D}, \mathbf{k}_{1D})$

$$\omega_{1D} = \omega_0 - \omega_{2D} \quad k_{1D} = \sqrt{\frac{2}{3}} \frac{\omega_0}{V_e} \sqrt{\delta} \quad (2b)$$

IAD: $(\omega_{2D}, \mathbf{k}_{2D})$

$$\omega_{2D} = \omega_0 \sqrt{\frac{2}{3}} \alpha \frac{V_i}{V_e} \sqrt{\delta} \quad \mathbf{k}_{2D} = -\mathbf{k}_{1D} \quad (2c)$$

LWC: $(\omega_{1C}, \mathbf{k}_{1C})$

$$\omega_{1C} = \omega_0 - (2c + 1)\omega_{2D} \quad \mathbf{k}_{1C} = (-1)^c \mathbf{k}_{1D} (c = 1, 2, \dots) \quad (2d)$$

IAC: $(\omega_{2C}, \mathbf{k}_{2C})$

$$\omega_{2C} = 2\omega_{2D} \quad \mathbf{k}_{2C} = (-1)^{c+1} 2\mathbf{k}_{1D} (c = 1, 2, \dots) \quad (2e)$$

LWG: $(\omega_{1G}, \mathbf{k}_{1G})$

$$\omega_{1G} = \omega_0 \quad k_{1G} = k_{1D} \quad (2f)$$

IAG: $(\omega_{2G}, \mathbf{k}_{2G})$

$$\omega_{2G} = 0 \quad k_{2G} = k_{1D} \quad (2g)$$

The relations (2b)–(2e) are derived in Appendix A. They relate to an unmagnetized plasma. In the above, $V_i \equiv (2KT_i/m_i)^{1/2}$ and $V_e \equiv (KT_e/m_e)^{1/2}$, where K is Boltzmann's constant, T_e and T_i are the electron and ion temperatures, and m_e and m_i are the electron and ion masses, respectively. The integer c denotes the order of the cascade product; $c = 1$ is thus the daughter of the primary Langmuir wave LWD. The parameter α is discussed in Appendix A and shown, as a function of T_e/T_i , in Figure A2. The wave number k_0 is much smaller than any of the other wave numbers and is therefore taken to be zero. In the above and in the following, the wave number k is defined as $|k|$ and is thus always a positive quantity.

In sections 3.2 to 3.4 we discuss the scatter processes by which the electrostatic waves given by (2b)–(2g) can be converted into electromagnetic waves.

3.2. Scattering of Langmuir Waves Into Electromagnetic Waves

The electric field of a Langmuir wave, $\mathbf{E}_1(\omega_1, \mathbf{k}_1)$, generates the electron velocity $\mathbf{v}_1(\omega_1, \mathbf{k}_1) = M(\omega_1) \mathbf{E}_1(\omega_1, \mathbf{k}_1)$, with M the electron mobility. In the presence of an electron density perturbation $N_2(\omega_2, \mathbf{k}_2)$, the current $\mathbf{j}(\omega_s, \mathbf{k}_s) = -\frac{1}{2}e M(\omega_1) N_2(\omega_2, \mathbf{k}_2) \mathbf{E}_1(\omega_1, \mathbf{k}_1)$ is produced, with

$$\omega_s = \omega_1 \pm \omega_2 \quad \mathbf{k}_s = \mathbf{k}_1 \pm \mathbf{k}_2 \quad (3)$$

where the subscript s stands for "scattered." If the scattered wave is electromagnetic, that is, $k_s \ll k_1, k_2$, the wave vector relation (3) requires

$$\mathbf{k}_1 = \mp \mathbf{k}_2 \quad (4)$$

That is, \mathbf{k}_1 and \mathbf{k}_2 have to be either parallel or antiparallel. Introducing the symbols $\uparrow\uparrow$ for parallel and $\uparrow\downarrow$ for antiparallel, we obtain for ω_s

$$\omega_s = \omega_1 + \omega_2 \quad \mathbf{k}_1 \uparrow\downarrow \mathbf{k}_2 \quad (5a)$$

$$\omega_s = \omega_1 - \omega_2 \quad \mathbf{k}_1 \uparrow\uparrow \mathbf{k}_2 \quad (5b)$$

The wave vector relation (4) can be satisfied by the following scatter processes.

LWD + IAD:

$$\omega_s = \omega_0 \quad (6a)$$

$$\omega_s = \omega_0 - 2\omega_{2D} \quad (6b)$$

LWD + IAG

$$\omega_s = \omega_0 - \omega_{2D} \quad (6c)$$

LWC + IAD:

$$\omega_s = \omega_0 - 2c\omega_{2D} \quad (6d)$$

$$\omega_s = \omega_0 - 2(c + 1)\omega_{2D} \quad (6e)$$

LWC + IAG:

$$\omega_s = \omega_0 - (2c + 1)\omega_{2D} \quad (6f)$$

LWG + IAD:

$$\omega_s = \omega_0 + \omega_{2D} \quad (6g)$$

$$\omega_s = \omega_0 - \omega_{2D} \quad (6h)$$

LWG + IAG:

$$\omega_s = \omega_0 \quad (6i)$$

We see that ion acoustic waves excited by the cascading process, IAC, are not able to participate in the scattering of Langmuir waves into electromagnetic waves. There is, however, the possibility that these waves are involved in a twofold scatter process. This will be investigated in the following section.

3.3. Scattering of Langmuir Waves Into Langmuir Waves

If the scattered and the scattering high frequency waves are Langmuir waves, $k_s = k_{1D}$ and $k_1 = k_{1D}$ have to be satisfied. If furthermore the scattering low-frequency wave has the wave number $k_2 = 2k_{1D}$, then the relation $\mathbf{k}_s = \mathbf{k}_1 \pm \mathbf{k}_2$ can only be satisfied if $\mathbf{k}_s = -\mathbf{k}_1$, and thus

$$\mathbf{k}_1 = \mp \frac{1}{2} \mathbf{k}_2 \quad (7)$$

Because of $\omega_2 = 2\omega_{2D}$ (see equation (2e)), the frequency of secondary Langmuir waves generated by scattering of primary Langmuir waves at the low frequency waves IAC is given by

$$\omega_s = \omega_1 + 2\omega_{2D} \quad \mathbf{k}_1 \uparrow \downarrow \mathbf{k}_2 \quad (8a)$$

$$\omega_s = \omega_1 - 2\omega_{2D} \quad \mathbf{k}_1 \uparrow \uparrow \mathbf{k}_2 \quad (8b)$$

Equations (8a) and (8b) are applicable to the following scatter processes:

LWD + IAC:

$$\omega_s = \omega_0 + \omega_{2D} \quad (9a)$$

$$\omega_s = \omega_0 - 3\omega_{2D} \quad (9b)$$

LWC + IAC:

$$\omega_s = \omega_0 - (2c - 1)\omega_{2D} \quad (9c)$$

$$\omega_s = \omega_0 - (2c + 3)\omega_{2D} \quad (9d)$$

LWG + IAC:

$$\omega_s = \omega_0 + 2\omega_{2D} \quad (9e)$$

$$\omega_s = \omega_0 - 2\omega_{2D} \quad (9f)$$

These Langmuir waves can now scatter into electromagnetic waves, following (5a) and (5b).

LWD + IAC + IAD:

$$\omega_s = \omega_0 + 2\omega_{2D} \quad (10a)$$

$$\omega_s = \omega_0 \quad (10b)$$

$$\omega_s = \omega_0 - 2\omega_{2D} \quad (10c)$$

$$\omega_s = \omega_0 - 4\omega_{2D} \quad (10d)$$

LWD + IAC + IAG:

$$\omega_s = \omega_0 + \omega_{2D} \quad (10e)$$

$$\omega_s = \omega_0 - 3\omega_{2D} \quad (10f)$$

LWC + IAC + IAD:

$$\omega_s = \omega_0 - 2(c - 1)\omega_{2D} \quad (10g)$$

$$\omega_s = \omega_0 - 2c\omega_{2D} \quad (10h)$$

$$\omega_s = \omega_0 - 2(c + 1)\omega_{2D} \quad (10i)$$

$$\omega_s = \omega_0 - 2(c + 2)\omega_{2D} \quad (10j)$$

LWC + IAC + IAG:

$$\omega_s = \omega_0 - (2c - 1)\omega_{2D} \quad (10k)$$

$$\omega_s = \omega_0 - (2c + 3)\omega_{2D} \quad (10l)$$

LWG + IAC + IAD:

$$\omega_s = \omega_0 + 3\omega_{2D} \quad (10m)$$

$$\omega_s = \omega_0 + \omega_{2D} \quad (10n)$$

$$\omega_s = \omega_0 - \omega_{2D} \quad (10o)$$

$$\omega_s = \omega_0 - 3\omega_{2D} \quad (10p)$$

LWG + IAC + IAG:

$$\omega_s = \omega_0 + 2\omega_{2D} \quad (10q)$$

$$\omega_s = \omega_0 - 2\omega_{2D} \quad (10r)$$

Since the lines described by (10a)–(10r) depend on a twofold scatter process, it is not obvious that they are strong enough to be of significance. We therefore have to go through some quantitative evaluation of the line strength. The field strength of the scattered wave E_s is inversely proportional to $|D_s|$, where D_s is the plasma dielectric function, given by

$$D_s(\text{EM}) = 1 - \frac{\omega_p^2}{\omega_s^2} - \frac{k_s^2 c^2}{\omega_0^2} + i \frac{\nu}{\omega_0} \quad (11a)$$

if the scattered wave is electromagnetic and

$$D_s(\text{LW}) = 1 - \frac{\omega_p^2}{\omega_s^2} - \frac{3k_s^2 V_e^2}{\omega_0^2} + i \frac{\nu}{\omega_0} \quad (11b)$$

if the scattered wave is a Langmuir wave. Here, ν is the electron collision frequency. At resonance, $|D_s| = \nu/\omega_0$, and thus

$$E_s \sim \frac{\omega_0}{\nu} \quad (12)$$

This relation has the shortcoming that it is based on the existence of two monochromatic waves that are either in resonance (in which case (12) is applicable) or not (in which case E_s becomes insignificant). Actually, however, the two interacting waves fill a finite interval in ω or k space, and so some of the wave couples will be in resonance, whereas others are not. What we have to do, therefore, in order to correct expression (12) is to multiply it with the number of resonant wave couples and divide it by the total number of couples. The latter is proportional to Δk_{1D} as given by (A12), while the first is proportional to the resonance width Δk_R , which is easily obtained from (11a) and (11b) with (1) as

$$\Delta k_R(\text{EM}) = \frac{\nu}{\sqrt{8} c \sqrt{\delta}} \quad (13a)$$

$$\Delta k_R(\text{LW}) = \frac{\nu}{\sqrt{24} V_e \sqrt{\delta}} \quad (13b)$$

The corrected expressions for (12) thus read

$$E_s(\text{EM}) \sim \frac{3}{\sqrt{8}} \frac{1}{\Delta\alpha} \frac{V_e^2}{\sqrt{\delta} c V_i} \quad (14a)$$

$$E_s(\text{LW}) \sim \frac{\sqrt{3}}{\sqrt{8}} \frac{1}{\Delta\alpha} \frac{V_e}{\sqrt{\delta} V_i} \quad (14b)$$

By comparison of (14a) and (14b) we conclude that scatter of a Langmuir wave into another Langmuir wave is by a factor $c/\sqrt{3}V_e$ more efficient than scatter of a Langmuir wave into an electromagnetic wave. The factor $c/\sqrt{3}V_e$ corresponds to approximately 60 dB. This means that a twofold scatter process (where the first step is scattering into LW and the second scattering into EM) is competitive with direct LW → EM scatter if the final scattering in the two-step process results in a loss of not more than 60 dB. This criterion can be easily checked, and we see from Figures 1–4 that it is usually fulfilled. Naturally, the observed field strengths do not only depend on the efficiencies of the processes involved, but likewise on the field strength of the high-frequency wave and the relative electron density perturbation of the low-frequency wave participating in the scatter process.

A by-product of the above considerations is that the efficiency of the scatter process increases as one approaches the pump wave reflection altitude, as can be seen from (14a) and (14b).

3.4. Scattering of the Electromagnetic Pump Wave Into Langmuir Waves

Having demonstrated that a twofold scatter process can be competitive, we should also consider the possibility of scattering of the pump wave into Langmuir waves with subsequent scattering into secondary electromagnetic waves.

If the scattering HF wave is electromagnetic, i.e., $k_1 = 0$, we obtain from (3)

$$\mathbf{k}_s = \pm \mathbf{k}_2 \quad (15)$$

$$\omega_s = \omega_0 + \omega_2 \quad \mathbf{k}_s \uparrow \uparrow \mathbf{k}_2 \quad (16a)$$

$$\omega_s = \omega_0 - \omega_2 \quad \mathbf{k}_s \uparrow \downarrow \mathbf{k}_2 \quad (16b)$$

Equations (16a) and (16b) are applicable to the following scatter processes:

EM + IAD:

$$\omega_s = \omega_0 + \omega_{2D} \quad (17a)$$

$$\omega_s = \omega_0 - \omega_{2D} \quad (17b)$$

EM + IAG:

$$\omega_s = \omega_0 \quad (17c)$$

The subsequent scattering of these Langmuir waves into secondary electromagnetic waves is possible through the following processes:

EM + IAD + IAD:

$$\omega_s = \omega_0 + 2\omega_{2D} \quad (18a)$$

$$\omega_s = \omega_0 \quad (18b)$$

$$\omega_s = \omega_0 - 2\omega_{2D} \quad (18c)$$

EM + IAD + IAG:

$$\omega_s = \omega_0 + \omega_{2D} \quad (18d)$$

$$\omega_s = \omega_0 - \omega_{2D} \quad (18e)$$

EM + IAG + IAG

$$\omega_s = \omega_0 \quad (18f)$$

In summarizing sections 3.2 to 3.4, we see that secondary electromagnetic waves are generated at the frequencies $\omega_0 + n\omega_{2D}$, where the integer n can take any value below and including 3, $n \leq 3$. It should be emphasized that ω_{2D} , given by (2c), is not a discrete quantity since it depends on δ , that is, on the distance from the reflection height of the O mode heating wave. Thus, the “lines” described by (6a)–(6i), (10a)–(10r), and (18a)–(18f) should primarily form a continuous spectrum, unless special reasons can be found why the contributions from distinct altitudes should dominate and thereby give rise to discrete features in the spectrum. This will be our next task.

3.5. Standing Wave Pattern of the Electromagnetic Pump Near the Reflection Point

The most obvious reason for having preferred altitude regions is given by the fact that the electromagnetic pump forms a standing wave. Naturally, the frequencies of waves originating at the locations of the Airy extrema are expected to dominate. The properties of the Airy function are summarized in Appendix B.

The frequency ω_{2D} adopts the following values at the Airy extrema, as can be derived from (2c), (B1b), (B3a), and (B3b).

$$\omega_{2D}(\zeta_m) = \omega_0 \frac{\alpha}{\sqrt{3}} \frac{V_i}{V_e} (k_0 H)^{-1/3} \left[\frac{3\pi}{4} \left(2m - \frac{3}{2} \right) \right]^{1/3} \quad (m \geq 2) \quad (19)$$

$$\omega_{2D}(\zeta_1) = \omega_0 \frac{\alpha}{\sqrt{3}} \frac{V_i}{V_e} (k_0 H)^{-1/3}$$

The first five values of $\omega_{2D}(\zeta_m)/\omega_0$ (for O^+ ions, $T_e/T_i = 2$, $f_0 \equiv \omega_0/2\pi = 5$ MHz, $H = 50$ km) are 2.96×10^{-4} , 5.35×10^{-4} , 6.51×10^{-4} , 7.36×10^{-4} , 8.05×10^{-4} , corresponding to the δ_m values 0.0017, 0.0054, 0.0080, 0.0102, 0.0122.

We can now argue that the discrete frequencies given by (19) will show up in the spectrum as discrete features if the difference between adjacent frequencies, $\omega_{2D}(\zeta_m) - \omega_{2D}(\zeta_{m-1})$, exceeds the frequency spread $\Delta\omega_{2D}$ given by (A11). By comparing the frequency values given above with the frequency spread following from Figure A2, we conclude that the frequency corresponding to the first Airy extremum, possibly also to the second, has a good chance to stand out as a discrete feature, while the other frequencies will be smeared out.

With increasing pump field strength E_0 , the gaps in δ space (around the Airy zeros) not filled with plasma waves will become smaller, and eventually even the first Airy peak will be smeared out. Conversely, discreteness will be supported if E_0 only slightly exceeds the threshold. We see from (B5) that the swelling factor ratio $s(\zeta_1)/s(\zeta_2) = 1.62$ is rather large, and there is thus the possibility that cases occur where the threshold is exceeded only at the first Airy maximum. When this happens, only waves with frequencies in the vicinity of $\omega_{2D}(\zeta_1)$ will be excited.

3.6. Threshold as a Function of Altitude

If the threshold of the parametric decay instability would turn out to be altitude dependent, then waves with frequencies corresponding to the altitude of the threshold minimum would be preferentially excited.

In the presence of an HF pump wave with frequency ω_0 , the dispersion relation of ion acoustic waves (ω, k) is given by (see,

e.g., *Fejer and Leer* [1972])

$$\frac{1}{D_i(k, \omega) - 1} + \frac{1}{D_e(k, \omega)} + \frac{1}{4} (\mathbf{k} \cdot \boldsymbol{\varepsilon})^2 \left[\frac{\omega_0}{2(\omega_0 + \omega - \omega_R) + i\nu} + \frac{\omega_0}{2(\omega_0 - \omega - \omega_R) - i\nu} \right] = 0 \quad (20)$$

with $\omega_R = (\omega_p^2 + 3k^2 V_e^2)^{1/2}$ the Langmuir wave resonance frequency and $\boldsymbol{\varepsilon} = -e\mathbf{E}_0/m\omega_0^2$ the excursion of an electron within the pump wave. Usually, one can neglect the first contribution in brackets (which impedes growth), because it lies outside the resonance of the second contribution. Then the threshold given by *Fejer* [1979],

$$E_{\text{oth}}^2 = \frac{4N_e K T_i}{\varepsilon_0} \frac{\nu}{\omega_0 B_{\text{max}}} \quad (21a)$$

results. B_{max} as a function of T_e/T_i is shown in Figure A1. If ω is not much larger than ν , the first contribution in brackets cannot be neglected, and the threshold has to be corrected according to

$$E_{\text{oth}}^2 = \frac{4N_e K T_i}{\varepsilon_0} \frac{\nu}{\omega_0 B_{\text{max}}} \left[1 - \frac{\nu^2}{(4\omega_{2D})^2 + \nu^2} \right]^{-1} \quad (21b)$$

In (21a) and (21b), ion collisions and losses by convection are neglected.

In the *F* region of the ionosphere, ν consists of two contributions, $\nu = \nu_{ei} + \nu_L$, denoting electron-ion collisions and Landau damping. These are given by the well-known expressions

$$\nu_{ei} = \omega_p (2/\pi)^{1/2} (12\pi N_e \lambda_D^3)^{-1} \ln(12\pi N_e \lambda_D^3) \quad (22a)$$

$$\nu_L = \omega_p (\pi/2)^{1/2} (k_{1D}^3 \lambda_D^3)^{-1} \exp[-3/2 - (2k_{1D}^2 \lambda_D^2)^{-1}] \quad (22b)$$

By relating N_e to ω_p (with $\omega_p \approx \omega_0$), taking k_{1D} and ω_{2D} from (A8a) and (A7), and reading B_{max} from Figure A1, we can evaluate the threshold as a function of altitude. Figure 6 shows E_{oth} versus δ for $T_i = 1000^\circ\text{K}$ and $f_0 = 3, 4.5, 6, 7.5$ MHz, with T_e/T_i as parameter. We notice that there does indeed exist a minimum. This, however, has the form of a

broad plateau, reaching from $\delta_{\text{min}} = 10^{-7}$ to 10^{-5} to $\delta_{\text{max}} = 5 \times 10^{-1}$, and thus a broad frequency band rather than a discrete frequency will be preferentially excited.

3.7. Height Integrated Stimulated Emission Intensities

The stimulated electromagnetic emission observed on the ground comes from the whole height range $\delta_{\text{min}} < \delta < \delta_{\text{max}}$ introduced at the end of the previous section. Any given frequency within the stimulated emission spectrum is generated within a finite height interval lying inside this height range. Clearly, the intensity of a wave with a given frequency will be the larger the wider the height interval from where it originates.

The height interval hereby defined is related to the frequency spreads of the waves involved in the respective scatter process. Let us now characterize a wave by three parameters, ω , $\Delta\omega^-$, and $\Delta\omega^+$, denoting the frequency, the downward frequency spread, and the upward frequency spread, respectively. Then the scatter process of the two waves $(\omega_1, \Delta\omega_1^-, \Delta\omega_1^+)$, $(\omega_2, \Delta\omega_2^-, \Delta\omega_2^+)$ will result in the scattered wave $(\omega_s, \Delta\omega_s^-, \Delta\omega_s^+)$, with $\omega_s, \Delta\omega_s^-, \Delta\omega_s^+$ given by

$$(\omega_s, \Delta\omega_s^-, \Delta\omega_s^+) = (\omega_1 + \omega_2, \Delta\omega_1^- + \Delta\omega_2^-, \Delta\omega_1^+ + \Delta\omega_2^+) \quad (23a)$$

or

$$(\omega_s, \Delta\omega_s^-, \Delta\omega_s^+) = (\omega_1 - \omega_2, \Delta\omega_1^- + \Delta\omega_2^+, \Delta\omega_1^+ + \Delta\omega_2^-) \quad (23b)$$

We furthermore define the quantities $\omega_s^+ \equiv \omega_s + \Delta\omega_s^+$, $\omega_s^- \equiv \omega_s - \Delta\omega_s^-$. In Figure 7 we have illustrated $\omega_s, \omega_s^+, \omega_s^-$ as a function of δ . We see from this illustration that the height interval $\Delta\delta \equiv \Delta\delta^- + \Delta\delta^+$ within which scattered waves of a given frequency are produced is related to the frequency spread through

$$\omega_s^-(\delta + \Delta\delta^+) = \omega_s(\delta) \quad (24a)$$

$$\omega_s^+(\delta - \Delta\delta^-) = \omega_s(\delta) \quad (24b)$$

if ω_s increases with δ and

$$\omega_s^+(\delta + \Delta\delta^+) = \omega_s(\delta) \quad (24c)$$

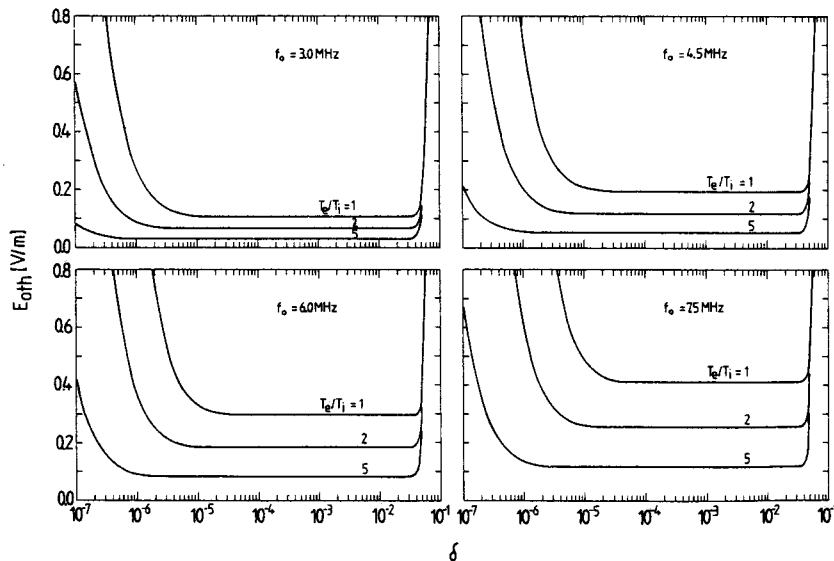


Fig. 6. Threshold field strength of the parametric decay instability as a function of δ , for three values of T_e/T_i and four values of the pump frequency, f_0 .

$$\omega_s^-(\delta - \Delta\delta^-) = \omega_s(\delta) \quad (24d)$$

if ω_s decreases with δ . As we shall see, ω_s and $\Delta\omega_x^\pm$ can be expressed in the form

$$\omega_s = \omega_0 + A\sqrt{\delta} \quad (25a)$$

$$\Delta\omega_s^\pm = B^\pm\sqrt{\delta} \quad (25b)$$

For $A > 0$ we have to use (24a) and (24b), and for $A < 0$ we have to use (24c) and (24d). In so doing, we obtain for $\Delta\delta^\pm$

$$\Delta\delta^+ = \left[\left(\frac{A}{A - B^-} \right)^2 - 1 \right] \delta \quad A > 0 \quad (26a)$$

$$\Delta\delta^- = \left[1 - \left(\frac{A}{A + B^+} \right)^2 \right] \delta \quad A > 0 \quad (26b)$$

and

$$\Delta\delta^+ = \left[\left(\frac{A}{A + B^+} \right)^2 - 1 \right] \delta \quad A < 0 \quad (26c)$$

$$\Delta\delta^- = \left[1 - \left(\frac{A}{A - B^-} \right)^2 \right] \delta \quad A < 0 \quad (26d)$$

We see from (26a)–(26d) that the height interval $\Delta\delta = \Delta\delta^+ + \Delta\delta^-$ in which waves with the frequency (25a) are generated is proportional to δ . Now we have to realize that $\delta + \Delta\delta^+$ must not exceed δ_{\max} . Taking this condition into account, we find that $\Delta\delta$ attains a maximum when $\delta + \Delta\delta^+ = \delta_{\max}$. Denoting by δ_M the altitude where this condition is satisfied, we obtain from (26a) and (26c) and (25a) and (25b)

$$\delta_M = \left(1 - \frac{B^-}{A} \right)^2 \delta_{\max} \quad A > 0 \quad (27a)$$

$$\delta_M = \left(1 + \frac{B^+}{A} \right)^2 \delta_{\max} \quad A < 0 \quad (27b)$$

The frequency ω_s generated at the altitude δ_M thus possesses the maximum height interval of generation, and correspondingly a maximum in the stimulated emission spectrum should appear at this frequency.

In order to be able to practically apply (27a) and (27b), we have to specify the frequency spreads of the waves involved in the scatter processes. This is easily done for the EM, IAD, LWD, IAG, and LWG waves, using (2b)–(2g) and (A11)

EM:

$$\Delta\omega_0^+ = 0 \quad \Delta\omega_0^- = 0 \quad (28a)$$

IAD:

$$\Delta\omega_{2D}^+ = \frac{\Delta\alpha^+}{\alpha} \omega_{2D} \quad \Delta\omega_{2D}^- = \frac{\Delta\alpha^-}{\alpha} \omega_{2D} \quad (28b)$$

LWD:

$$\Delta\omega_{1D}^+ = \Delta\omega_{2D}^- \quad \Delta\omega_{1D}^- = \Delta\omega_{2D}^+ \quad (28c)$$

IAG:

$$\Delta\omega_{2G}^+ \approx 0 \quad \Delta\omega_{2G}^- \approx 0 \quad (28d)$$

LWG:

$$\Delta\omega_{1G}^+ \approx 0 \quad \Delta\omega_{1G}^- \approx 0 \quad (28e)$$

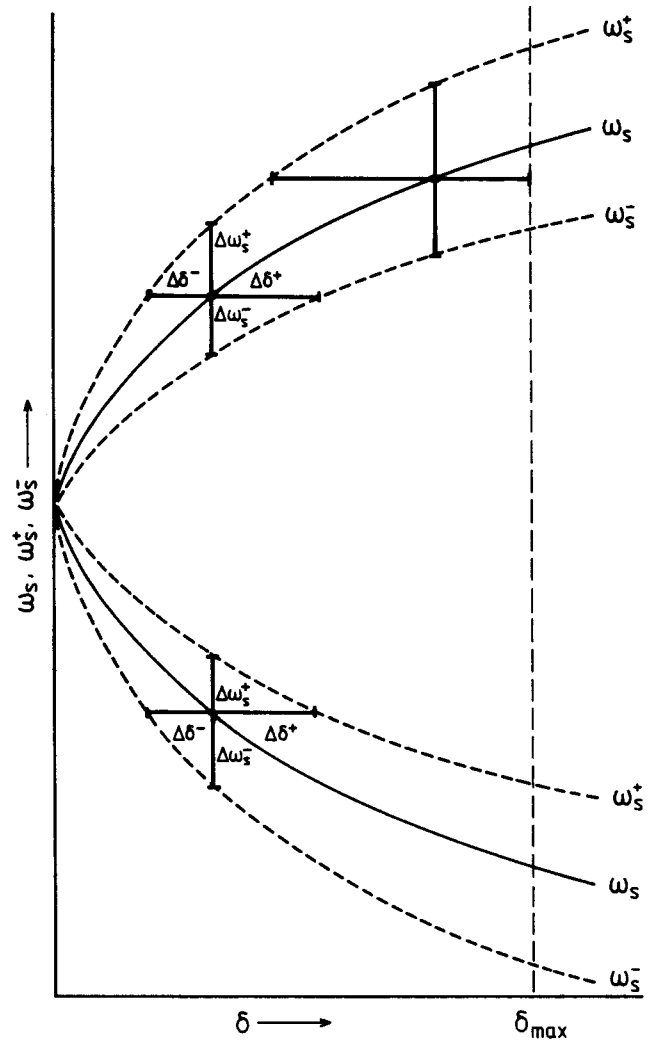


Fig. 7. Sketch to illustrate the relationship between height spread and frequency spread.

If we take $\Delta\alpha^+$ as the difference between the upper and middle curve in Figure A2, and $\Delta\alpha^-$ as the difference between the middle and lower curve, then the frequency spreads given by (28b) and (28c) relate to the case $E_0^2 = 2E_{\text{oth}}^2$. A larger (smaller) frequency spread results if E_0 is larger (smaller) than this value.

Once E_0 is specified, the field strengths of the LWD and LWC waves follow self-consistently, and thus the frequency spreads of the cascade products are obtained from saturation theory. It is beyond the scope of this paper to go through such an involved investigation. Certain hints, however, can be obtained from a simplified saturation theory, which is presented in Appendix C. From (C10) and (C9)

IAC:

$$\Delta\omega_{2D}^\pm \leq \Delta\omega_{2C}^\pm \leq 2\Delta\omega_{2D}^\pm \quad c = 1 \quad (28f)$$

LWC:

$$\Delta\omega_{2D}^\mp \leq \Delta\omega_{1C}^\pm \leq 2\Delta\omega_{2D}^\mp \quad c = 1 \quad (28g)$$

In summarizing sections 3.5 to 3.7, we have identified two mechanisms through which spectral contributions from distinct altitudes could be dominant. One is the altitude corresponding to the first Airy maximum, and the resulting fre-

quency is given by (19). The other is the altitude where the height interval within which a wave of given frequency is generated has a maximum. The corresponding frequency follows from (27a, b). We shall have to see now whether these mechanisms are indeed able to explain the experimental findings presented in section 2.

4. DISCUSSION

In this section we intend to use the relationships established in section 3 in order to interpret the experimental findings presented in section 2.

4.1. The Continuum

The continuum is a strong and regular spectral feature, and we should therefore try to explain it in terms of the strongest products of the parametric decay instability, i.e., through the scatter process LWD + IAD. From (6a), (6b), (23), and (28c), we obtain

$$\omega_s = \omega_0 \quad \Delta\omega_s^- = \Delta\omega_{2D}^- + \Delta\omega_{2D}^+ \quad \Delta\omega_s^+ = \Delta\omega_s^- \quad (29a)$$

$$\omega_s = \omega_0 - 2\omega_{2D} \quad \Delta\omega_s^- = 2\Delta\omega_{2D}^+ \quad \Delta\omega_s^+ = 2\Delta\omega_{2D}^- \quad (29b)$$

The first contribution, described by (29a), is symmetric around ω_0 ,

$$-\Delta\omega_{2D}^- - \Delta\omega_{2D}^+ \leq \omega_s - \omega_0 \leq \Delta\omega_{2D}^- + \Delta\omega_{2D}^+ \quad (30a)$$

whereas the second contribution, described by (29b), only contributes to the downshifted portion of the spectrum,

$$-2(\omega_{2D} + \Delta\omega_{2D}^+) \leq \omega_s - \omega_0 \leq -2(\omega_{2D} - \Delta\omega_{2D}^-) \quad (30b)$$

The largest frequency range occupied by these secondary electromagnetic waves is thus

$$-2(\omega_{2D} + \Delta\omega_{2D}^+) \leq \omega_s - \omega_0 \leq \Delta\omega_{2D}^- + \Delta\omega_{2D}^+ \quad (30c)$$

with ω_{2D} , $\Delta\omega_{2D}^\pm$ relating to δ_{\max} , i.e., the largest possible value of δ . Taking $\delta_{\max} = 0.05$ (see Figure 6) and, to give an example, $T_e/T_i = 2$ and $E_0^2 = 2E_{0th}^2$, we obtain from Figures A2 and A3

$$-4 \times 10^{-3} \times f_0 \leq \Delta f \leq 0.9 \times 10^{-3} f_0 \quad (30d)$$

with $\Delta f \equiv (\omega_s - \omega_0)/2\pi$ and $f_0 \equiv \omega_0/2\pi$. This is indeed the right order of magnitude. We have to realize, however, that the frequency range becomes larger (smaller) for smaller (larger) T_e/T_i and larger (smaller) E_0^2/E_{0th}^2 . Furthermore, the asymmetry between the upshifted and downshifted portions of the continuum becomes more (less) pronounced for larger (smaller) T_e/T_i and smaller (larger) E_0^2/E_{0th}^2 .

The width given by (30c) and (30d) is an upper limit that is not reached if, owing to swelling, the threshold is exceeded only in the vicinity of the reflection height. This seems to be the case in Figure 1a. On the other hand, the spectra shown in Figures 1c and 1d are wider and more asymmetric than could possibly be explained by (30c), even if we choose more favorable values for T_e/T_i and E_0^2/E_{0th}^2 than those leading to (30d). It appears, therefore, that occasionally other processes participate in the generation of the continuum. A plausible extension of (29a) and (29b) is to invoke the cascade products, i.e., the processes LWC + IAD (see equations (6d) and (6e)), LWD + IAC + IAD (see equation (10d)) and LWC +

IAC + IAD (see equations (10g)–(10j)). With these processes, the downshifted end of the spectrum becomes primarily a function of the number of excited cascade products. It is important to note that the upshifted end of the spectrum is not affected by processes involving cascade products, and the right-hand inequalities (equations (30c) and (30d)) therefore remain valid. This is indeed confirmed by all our measurements, including those shown in Figure 1.

The shape of the continuum, that is, the increase of the spectral intensity with decreasing Δf , should be mainly a consequence of (14a), $E_s \sim \delta^{-1/2}$. Another important factor is the swelling of the pump wave, which also favors contributions from small δ , that is, small offset frequencies.

4.2. The DM Feature

Next to the continuum, the DM is the most regular spectral feature. If we again primarily invoke the scatter process LWD + IAD, we arrive at (29b). The alternative (29a) is not useful here because it yields a spectral peak at ω_0 . If we now continue the discussion of the spectral shape of the continuum by incorporating the height spread effect discussed in section 3.7, we obtain a spectral maximum at the frequency

$$\omega_s = \omega_0 - 2\omega_{2D}(\delta_M) \quad (31a)$$

$$\delta_M = \left(1 - \frac{\Delta\alpha^-}{\alpha}\right)^2 \delta_{\max} \quad (31b)$$

(see (27b), (28b), (29b)). This maximum appears as an enhanced portion of the continuum. From (31a), (31b), and (2c)

$$\Delta f_{DM} = -f_0 \sqrt{\frac{8}{3}} (\alpha - \Delta\alpha^-) \frac{V_i}{V_e} \sqrt{\delta_{\max}} \quad (31c)$$

Since α , $\Delta\alpha^-$, and δ_{\max} depend on T_e/T_i and E_0/E_{0th} , and V_i/V_e depends on T_e/T_i and the ion composition, Δf_{DM} will depend to some extent on the experimental conditions. This is indeed observed. To give an example, we have found Δf_{DM} to range from -13 to -8 kHz for $f_0 = 5.423$ MHz. The curve labeled "theory" in Figure 5,

$$\Delta f_{DM} = -2 \times 10^{-3} f_0 \quad (31d)$$

is obtained for $\delta_{\max} = 0.05$, $E_0^2/E_{0th}^2 = 2$, $T_e/T_i = 2$ and $M_i = 16$ (O^+ ions).

Usually, the DM is the first discrete feature in the spectrum to show up, and the other discrete features are usually accompanied by the DM. Occasionally, however, other discrete features are visible while the DM is missing. One such case is depicted by Figure 4d. The explanation of the DM given here is based on the existence of LWD and IAD waves. Since none of the other features can be understood if these waves are not present, as we shall see, we cannot conclude that the absence of the DM is due to the absence of LWD and IAD waves. At this stage we should recall that the line (29b) on which the existence of the asymmetric part of the continuum and the DM is based requires LWD and IAD waves propagating in the same direction. Now we know that the decay instability produces LWD and IAD waves propagating in opposite directions. This as such does not matter since there is no a priori reason to assume that the intensity of excited LWD or IAD waves should change upon reversing their k vectors. From observations with the EISCAT incoherent scatter radar we know, however, that sometimes directional asymmetries in the heater produced plasma lines and enhanced ion line shoulders by as much as 20 dB occur [Kohl et al., 1983]. When this is

so, then the line (29b) should disappear or at least be drastically weakened, while the line (29a) remains unaffected. We suggest, therefore, that the disappearance of the DM and the asymmetric part of the continuum during the presence of other spectral features is due to directional asymmetries in the excitation of the primary products of the decay instability.

We should add for completeness that the lines (6d), (6e), (10c), (10g), (10h), (10k), (10r), and (18c) also contribute to the DM, but clearly the contribution from (6b) should dominate because it involves the primary products of the decay instability in a single scatter process.

4.3. The UM Feature

The upshifted maximum occurs at or closely to the mirror frequency of the DM, and it should therefore be explained in terms of lines at $\omega_0 + 2\omega_{2D}$. We see from sections 3.2 to 3.4 that such lines cannot be directly produced by the strongest decay products, and it is therefore immediately obvious that the UM should be significantly weaker than the DM. Among the three relevant processes, that is, LWD + IAC + IAD, LWG + IAC + IAG, EM + IAD + IAD, the second should be ruled out because it involves waves that are supposedly considerably weaker than the LWD, EM, and IAD waves. Let us first consider the scatter process LWD + IAC + IAD. From (10a), (23), (28c), we obtain

$$\begin{aligned} \omega_s &= \omega_0 + 2\omega_{2D} & \Delta\omega_s^- &= \Delta\omega_{2D}^- + \Delta\omega_{2D}^+ + \Delta\omega_{2C}^- \\ & & \Delta\omega_s^+ &= \Delta\omega_{2D}^- + \Delta\omega_{2D}^+ + \Delta\omega_{2C}^+ \end{aligned} \quad (32)$$

Correspondingly, for the scatter process EM + IAD + IAD from (18a) and (23)

$$\omega_s = \omega_0 + 2\omega_{2D} \quad \Delta\omega_s^- = 2\Delta\omega_{2D}^- \quad \Delta\omega_s^+ = 2\Delta\omega_{2D}^+ \quad (33)$$

The UM described by (33) corresponds fully to the DM described by (29b), and from (27a) and (28b) we obtain for this contribution

$$\Delta f_{UM}^{(1)} = f_0 \sqrt{\frac{8}{3}} (\alpha - \Delta\alpha^-) \frac{V_i}{V_e} \sqrt{\delta_{max}} = -\Delta f_{DM} \quad (34)$$

For the second contribution to the UM, described by (32), the relations (27a), (28b), and (28f) yield

$$\Delta f_{UM}^{(2)} = f_0 \sqrt{\frac{8}{3}} \left(\alpha - \frac{(1 + \alpha)\Delta\alpha^- + \Delta\alpha^+}{2} \right) \frac{V_i}{V_e} \sqrt{\delta_{max}} \quad (35)$$

with $1 \leq a \leq 2$ (see equation (28f)). From (34) and (35)

$$\Delta f_{UM}^{(2)}/\Delta f_{UM}^{(1)} = 1 - \frac{(a - 1)\Delta\alpha^- + \Delta\alpha^+}{2(\alpha - \Delta\alpha^-)} \quad (36)$$

For $T_e/T_i = 2$, $E_0^2/E_{0th}^2 = 2$ and $1 \leq a \leq 2$, we find $0.65 \leq \Delta f_{UM}^{(2)}/\Delta f_{UM}^{(1)} \leq 0.86$ which is in excellent agreement with observation.

4.4. The nDM Feature ($n \geq 2$)

There are several processes able to produce spectral maxima around multiples of the DM, in conjunction with the height spread effect discussed in section 3.7. These are LWC + IAD (equations (6d) and (6e)), LWD + IAC + IAD (equation (10d)), and LWC + IAC + IAD (equations (10g)–(10j)). In view of the multiplicity of possibilities and of the limited knowledge about the frequency spreads of the cascade products LWC and IAC, we refrain from discussing these pro-

cesses in detail. We can state, however, that the nDM maxima can be understood by scatter processes involving the cascade products of the parametric decay instability. There is no reason to assume that this phenomenon is restricted to $n = 2$ and $n = 3$, as observed. We would most likely obtain higher order maxima if a lower noise receiver and a higher gain antenna would be used.

We should also add that spectral maxima with $n = (2j + 1)/2$ ($j = 1, 2, \dots$) are predicted by the processes LWC + IAG (equation (6f)), LWD + IAC + IAG (equation (10f)), LWC + IAC + IAG (equations (10k) and (10l)), and LWG + IAC + IAD (equation (10p)). Furthermore, a $\frac{3}{2}$ UM feature is predicted by (10m) through the process LWG + IAC + IAD. A convincing experimental proof for these features, however, is lacking. Occasionally, we see vague indications of a $\frac{3}{2}$ DM.

4.5. The $\frac{1}{2}$ DM and $\frac{1}{2}$ UM Features

Lines at $\omega_0 \pm \omega_{2D}$ are generated by the processes LWD + IAG (equation (6c)), LWG + IAD (equations (6g) and (6h)), LWD + IAC + IAG (equation (10e)), LWC + IAC + IAG (equation (10k)), LWG + IAC + IAD (equations (10n) and (10o)) and EM + IAD + IAG (equations (18d) and (18e)). We concentrate our attention on the first two processes that are single scatter processes.

For the process LWD + IAG (equation (6c)), we obtain with (23) and (28c),

$$\omega_s = \omega_0 - \omega_{2D} \quad \Delta\omega_s^- = \Delta\omega_{2D}^+ \quad \Delta\omega_s^+ = \Delta\omega_{2D}^- \quad (37)$$

and correspondingly for the process LWG + IAD (equations (6g) and (6h)) with (23)

$$\omega_s = \omega_0 - \omega_{2D} \quad \Delta\omega_s^- = \Delta\omega_{2D}^+ \quad \Delta\omega_s^+ = \Delta\omega_{2D}^- \quad (38a)$$

$$\omega_s = \omega_0 + \omega_{2D} \quad \Delta\omega_s^- = \Delta\omega_{2D}^- \quad \Delta\omega_s^+ = \Delta\omega_{2D}^+ \quad (38b)$$

The frequencies of the $\frac{1}{2}$ DM and $\frac{1}{2}$ UM follow from (27a), (27b), and (28b) as

$$\begin{aligned} \Delta f_{1/2DM} &= -f_0 \sqrt{\frac{2}{3}} (\alpha - \Delta\alpha^-) \frac{V_i}{V_e} \sqrt{\delta_{max}} \\ &= \frac{1}{2} \Delta f_{DM} \end{aligned} \quad (39a)$$

$$\begin{aligned} \Delta f_{1/2UM} &= f_0 \sqrt{\frac{2}{3}} (\alpha - \Delta\alpha^-) \frac{V_i}{V_e} \sqrt{\delta_{max}} \\ &= -\Delta f_{1/2DM} = \frac{1}{2} \Delta f_{UM}^{(1)} \end{aligned} \quad (39b)$$

If the process LWD + IAG is stronger than the process LWG + IAG, then the $\frac{1}{2}$ DM should be stronger than the $\frac{1}{2}$ UM. If the process LWG + IAG dominates, then the $\frac{1}{2}$ DM and the $\frac{1}{2}$ UM should be equally strong. It is not possible within the frame of the explanation given here that the $\frac{1}{2}$ UM becomes stronger than the $\frac{1}{2}$ DM. This is in agreement with observation.

4.6. The DP and UP Features

The discrete features discussed in sections 4.2 to 4.5 all depend on the same physical mechanism: The frequency of the

respective spectral maximum is given by the condition that the height interval in which that particular frequency is generated maximizes, thereby making the height integrated intensity maximum. That such maximum exists is the result of Landau damping.

The lowest possible discrete features that can thereby be explained are the $\frac{1}{2}$ DM and $\frac{1}{2}$ UM. We now turn to the other mechanism capable of producing discrete spectral features, discussed in section 3.5, that is, we try to consider the DP and UP as signatures of the first Airy maximum. From the foregoing we know that the strongest downshifted and upshifted lines are those producing the DM and UM, $\omega_s = \omega_0 \pm 2\omega_{2D}$. Using (19), we immediately obtain

$$\Delta f_{DP} = -f_0 \sqrt{\frac{4}{3}} \alpha \frac{V_i}{V_e} (k_0 H)^{-1/3} \quad (40a)$$

$$\Delta f_{UP} = -\Delta f_{DP} \quad (40b)$$

Interestingly, the splitting of the UM does not occur in the UP, simply because the frequency spread of the lines is not relevant here in determining the peak frequency. Figure 8 shows Δf_{DP} and Δf_{UP} versus f_0 for various values of T_e/T_i and H (electron density scale height), assuming O^+ ions. The measured values for Δf_{DP} and Δf_{UP} lie fully within the range of values predicted by Figure 8.

The fact that the DP and UP features have a preference for the heating frequency 4.04 MHz, in comparison with 4.9128 and 5.423 MHz, is difficult to understand. Whether or not the first Airy maximum gives rise to a discrete spectral feature depends on the relation of the frequency difference $\omega_{2D}(\zeta_2) - \omega_{2D}(\zeta_1)$ to the frequency spread $\Delta\omega_{2D} = \Delta\omega_{2D}^- + \Delta\omega_{2D}^+$. A small value of the latter in relation to the first supports discreteness. A small frequency spread is obtained for small E_0^2/E_{0th}^2 . One could argue that HF waves with lower frequencies experience heavier absorption in the D region and that therefore their E_0^2/E_{0th}^2 is smaller than for HF waves with higher frequencies. Although this argument is certainly correct, it is nonetheless difficult to see how it could fully account for the experimental findings. Further investigations concerning the DP and UP features appear necessary.

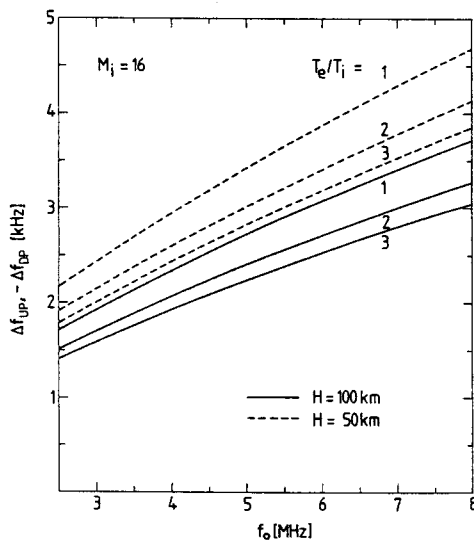


Fig. 8. Offset frequencies of the DP and UP, Δf_{DP} and Δf_{UP} , as a function of heating frequency, f_0 , for three values of T_e/T_i and two values of H . The ion gas is assumed to consist of O^+ , $M_i = 16$.

5. COMPARISON OF THE STIMULATED EMISSION AND INCOHERENT SCATTER TECHNIQUES

1. The fundamental difference between the two techniques is the fact that the incoherent scatter technique (IST) sees the individual plasma waves directly, while the stimulated emission technique (SET) sees the results of interaction between at least two such plasma waves. Therefore, a direct correspondence between the lines seen by the IST and the discrete features seen by the SET is not given. In particular, the distinction between high-frequency plasma lines and low-frequency ion lines pertinent to the IST does not apply to the SET, which only sees high-frequency features.

2. The SET is sensitive to all plasma waves excited in the medium, no matter which wavelength and propagation direction they have. The IST, on the other hand, only sees plasma waves with a wave vector \mathbf{k} satisfying the Bragg condition $\mathbf{k} = 2\mathbf{k}_R$, where \mathbf{k}_R is the radar wave vector. The Bragg condition in this form relates to monostatic radar operation. Thus only plasma waves excited at one particular altitude with propagation parallel or antiparallel to the radar beam are seen by the radar. This is a severe limitation of the IST.

3. The plasma waves may propagate during their lifetimes to satisfy the Bragg condition at a remote location. This propagation depends sensitively upon inhomogeneities in the medium, for example, plasma density irregularities due to natural causes or induced by the heater. The temporal development of the lines seen by the IST is therefore not a reliable indicator of the temporal development of the parametric instabilities involved. The SET, on the other hand, is rather insensitive to density irregularities.

4. Landau damping plays a widely different role for the SET and IST. While it is responsible for most of the discrete features seen by the SET and thus has a helpful function in identifying distinct plasma processes, it can annihilate the plasma and ion lines seen by the IST if the radar frequency is too high. The plasma waves in question either have the wave number k_{1D} (LWD, LWC, LWG, IAD, IAG, LWD + IAC, LWG + IAC, EM + IAD, EM + IAG) or the wave number $2k_{1D}$ (IAC). With (2b) and the Bragg condition, the altitude δ_R where a radar with frequency f_R detects plasma waves with wave number k_{1D} is given by

$$\delta_R = 6 \frac{V_e^2}{c^2} \frac{f_R^2}{f_0^2} = 10^{-6} \left(\frac{T_e}{1000} \right) \frac{f_R^2}{f_0^2} \quad (41)$$

The condition $\delta_R < \delta_{max}$, with $\delta_{max} \approx 0.05$, yields

$$\frac{f_R^2}{f_0^2} < 5 \times 10^4 \frac{1000}{T_e} \quad (41a)$$

To give an example, for $T_e = 2000^\circ\text{K}$ and $f_0 = 5$ MHz, f_R has to be less than 790 MHz, and so in this case the EISCAT UHF radar ($f_R = 933$ MHz) would not see plasma lines with wave number k_{1D} .

For IAC waves, which have the wave number $2k_{1D}$, the corresponding condition reads

$$\frac{f_R^2}{f_0^2} < 2 \times 10^5 \frac{1000}{T_e} \quad (41b)$$

which is satisfied, again for $T_e = 2000^\circ\text{K}$ and $f_0 = 5$ MHz, for f_R less than 1580 MHz.

An interesting consequence of these considerations is that cases can occur where the only lines seen by the IST are the enhanced ion line shoulders due to ion acoustic waves generated by the cascade process, while all other lines are absent.

5. The discrete features seen by the SET are mixed products of different modes of the parametric decay instability. There are, however, two discrete features that nonetheless correspond closely to lines seen by the IST. These correspondences are DM (LWD + IAD) and decay line (LWD), UM (EM + IAD + IAD, LWD + IAC + IAD), and image decay line (EM + IAD, LWD + IAC). Thus the DM and UM features appear well suited for comparative studies between the stimulated emission and incoherent scatter techniques. The UM has the advantageous property that the two competing processes producing the UM appear at different frequencies, whereas they cannot be resolved in the image decay line. Another, however less direct, correspondence exists between the $\frac{1}{2}$ UM (LWG + IAD) and the purely growing line (LWG). Finally, there is a certain correspondence between the n DM ($n = 2, 3, \dots$) and the cascade lines, which however is only loosely defined in view of the multiplicity of processes contributing to the n DM. The DP and UP do not have any correspondence in the incoherent scatter spectrum.

Altogether we see that each of the two techniques has certain advantages that complement each other ideally. A joint use of these techniques for the study of parametric instabilities is therefore highly commendable. It should not be forgotten to mention that the SET is by orders of magnitude less costly than the IST and could therefore be used at places where an incoherent scatter facility does not exist or is not available at demand.

6. EXPERIMENTAL RESULTS (SECOND PART)

In addition to those spectral features that can be interpreted by the mechanisms discussed in section 3, there are others that so far are poorly understood. These features will now be briefly presented.

1. Broad upshifted and downshifted maximum (BUM, BDM): Occasionally we observe a very strong upshifted spectral feature that extends up to 160 kHz above the carrier. It possesses a maximum at a frequency ranging from 20 to 40 kHz. Sometimes a second maximum occurs at twice this frequency. We call this feature the broad upshifted maximum (BUM). Examples of the BUM are shown in Figure 9. A strongly developed BUM is often accompanied by a much weaker BDM (broad downshifted maximum), also shown in Figure 9. Unlike the BUM, which is a very stable feature, the BDM shows a strong temporal variability. The peak frequency of the BDM sometimes corresponds to that of the BUM, but at other times the two peak frequencies are significantly different. It is therefore not clear yet whether or not the BUM and BDM are manifestations of the same physical process. All we can say in this respect is that the BDM occurs simultaneously with the BUM. In the initial stage of our experiments, when we randomly used all of the licensed heating frequencies (11 frequencies in the range 2.759 to 7.953 MHz), we had the impression that the BUM is a rare feature. In the meantime we have learned that the BUM is almost as regular as the DM provided the heating frequency lies within approximately 0.5 MHz below the O mode critical F region frequency. When we approach this condition, the BUM and BDM increase much faster than the DM and the other features introduced in section 2. It is therefore obvious that a plasma wave not included in the list (equations (2a)–(2g)) must participate in the formation of the BUM and BDM. A scatter process involving Langmuir waves generated by energetic electrons and IAC waves, or a double scatter process of these Langmuir waves with IAD waves would explain certain features of the

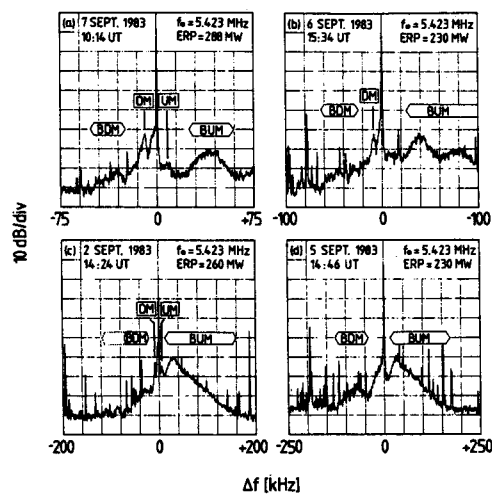


Fig. 9. Spectra to demonstrate the BUM and BDM features. Also seen are the DM and UM features. Further text as in Figure 1.

BUM, but there are reasons which make this an unlikely explanation.

2. Recently, we discovered another spectral feature, consisting of peaks at approximately 500 Hz below and above the carrier. This shoulderlike phenomenon is shown in Figure 10. Typically, the left shoulder is more strongly developed than the right. Further experiments are needed to sufficiently document the occurrence of the shoulder feature in relation to the other spectral features. A theoretical explanation has not yet been found.

3. Another recent finding was the occasional appearance of lines at approximately $1/3$, $2/3$ and $5/3$ times the 50 Hz mains frequency. Figure 11b shows an example of this. For comparison, Figure 11a shows a spectrum where these lines are absent, in order to demonstrate that they are not radiated by the heater. The lines at $16\frac{2}{3}$ Hz and multiples thereof could be the result of cross modulation between the heating wave and ELF waves unintentionally radiated by Swedish railway system.

7. CONCLUSIONS

A powerful electromagnetic O mode HF wave with a frequency below the F region critical frequency stimulates the emission of secondary electromagnetic waves. The stimulated emission spectrum is found to be richly structured. The observed spectral features are presented in two portions. The first portion deals with those features that we find theoretically explainable. The explanation involves single- and double-scatter processes among the diverse high-frequency Langmuir waves and low-frequency ion acoustic waves that are excited

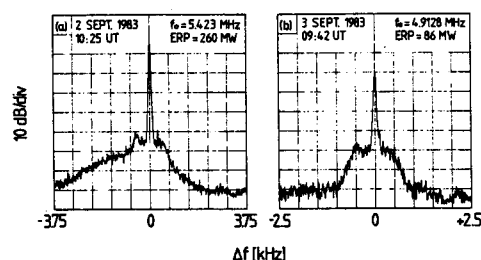


Fig. 10. Spectra to demonstrate the occurrence of maxima at $\Delta f \approx \pm 500$ Hz. Further text as in Figure 1.

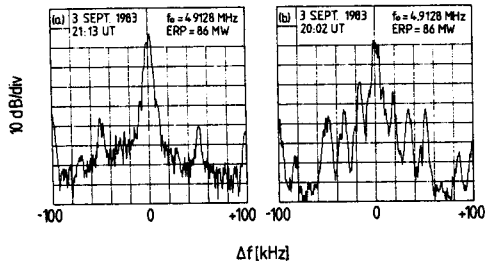


Fig. 11. Spectra to demonstrate the occasional occurrence of lines as 1/3, 2/3 and 5/3 times the 50 Hz mains frequency. Further text as in Figure 1.

by the parametric decay instability, including its purely growing mode, that is the oscillating two stream instability.

The theory presented is far from being complete. The aim was to understand the observed spectral features in the sense of linking them to well-defined physical processes. This aim appears to be reached, with certain reservations regarding the DP and UP features. It will now be a rewarding task to develop a quantitative theory to describe the stimulated emission spectrum.

The second portion of experimental results does not follow this theoretical explanation. Additional physical processes are called for. It appears to be a highly promising task to come to an understanding of these experimental findings. Particularly the broad upshifted maximum (BUM), once understood, is expected to reveal exciting new phenomena.

APPENDIX A: FREQUENCIES AND WAVE NUMBERS OF PARAMETRICALLY EXCITED PLASMA WAVES

The frequencies and wave vectors of the mother wave (ω_0 , \mathbf{k}_0) and the two electrostatic daughter waves (ω_1 , \mathbf{k}_1), (ω_2 , \mathbf{k}_2) involved in a parametric three wave process are related through the well-known selection rules

$$\omega_0 = \omega_1 + \omega_2 \quad \mathbf{k}_0 = \mathbf{k}_1 + \mathbf{k}_2 \quad (\text{A1})$$

We use suffix 1 for Langmuir waves and suffix 2 for ion acoustic waves.

The two HF waves (ω_0 , \mathbf{k}_0) and (ω_1 , \mathbf{k}_1) give rise to a ponderomotive force at $(\omega_0 - \omega_1, \mathbf{k}_0 - \mathbf{k}_1) \equiv (\omega_2, \mathbf{k}_2)$, which may enhance low-frequency plasma density perturbations (ω_2 , \mathbf{k}_2). The mother wave, interacting with the electron density perturbation (ω_2 , \mathbf{k}_2), generates a current at $(\omega_0 - \omega_2, \mathbf{k}_0 - \mathbf{k}_2) = (\omega_1, \mathbf{k}_1)$, and energy is thereby exchanged between the HF mother and the HF daughter. The power gain per unit volume and time of the HF daughter wave is given by Fejer [1979, equation (27)],

$$P_G = \frac{\omega_0 \epsilon_0^2}{8N_e K T_i} \left(\frac{E_0 \cdot \mathbf{k}_1}{E_0 k_1} \right)^2 E_0^2 E_1^2 B(\alpha, T_e/T_i) \quad (\text{A2})$$

where use has been made of $\omega_0 \approx \omega_p$. The function $B(\alpha, T_e/T_i)$ is specified by (18) and illustrated by Figure 3 of Fejer [1979], with α defined by

$$\alpha \equiv \frac{\omega_0 - \omega_1}{|\mathbf{k}_0 - \mathbf{k}_1| \cdot V_i} \quad V_i \equiv (2KT_i/m_i)^{1/2} \quad (\text{A3})$$

The function B has the property $B(-\alpha) = -B(\alpha)$, and thus the HF daughter wave can grow only if $\omega_0 > \omega_1$. A further property of B is that it possesses one maximum, and it is

plausible to assume that maximum growth occurs if α adopts the value $\alpha(B_{\max})$ which belongs to this maximum. We have recalculated $B(\alpha, T_e/T_i)$ and show in Figure A1 B_{\max} versus T_e/T_i , and in Figure A2 $\alpha(B_{\max})$ and $\alpha(0.5 B_{\max})$ versus T_e/T_i . The difference between the upper and lower $\alpha(0.5 B_{\max})$ values is a measure of the width of $B(\alpha)$ for a given T_e/T_i .

The real part of the Langmuir wave dispersion relation remains almost unaffected by the presence of the pump wave and is thus given by

$$\omega_1^2 = \omega_p^2 + 3k_1^2 V_e^2 \quad V_e^2 \equiv KT_e/m_e = \lambda_D^2 \omega_p^2 \quad (\text{A4})$$

with λ_D the Debye length. Using (1) together with $\omega_1 + \omega_0 \approx 2\omega_0$, we obtain from (A4)

$$\omega_0 - \omega_1 = \omega_0 \delta - \frac{3}{2} \frac{k_1^2 V_e^2}{\omega_0} \quad (\text{A5})$$

The frequency of parametrically excited ion acoustic waves, $\omega_2 = \omega_0 - \omega_1$, follows from (A3),

$$\omega_2 = \alpha |\mathbf{k}_0 - \mathbf{k}_1| V_i \quad (\text{A6})$$

The range of values for α depends on E_0 , that is, the pump field strength. At threshold, $E_0^2 = E_{0\text{th}}^2$, α can only take the value $\alpha(B_{\max})$ as given by the central curve in Figure A2, while for $E_0^2 = 2E_{0\text{th}}^2$, α can take any value between the lower and upper curve in Figure A2. In general, the range of values for α increases with E_0 .

In applying (A6) to the primary decay products, LWD and IAD, we make use of $k_0 = 0$, and thus have

$$\omega_{2D} = \alpha k_{1D} V_i \quad (\text{A7})$$

By combining (A5) and (A7), we obtain

$$k_{1D} = \sqrt{\frac{2}{3}} \frac{\omega_0}{V_e} [\sqrt{\delta + \bar{\delta}} - \sqrt{\bar{\delta}}] \quad (\text{A8a})$$

with

$$\bar{\delta} = \alpha^2 V_i^2 / 6V_e^2 \quad (\text{A8b})$$

$\bar{\delta}$ is on the order 10^{-5} . For $\delta \gg \bar{\delta}$, which is satisfied except at

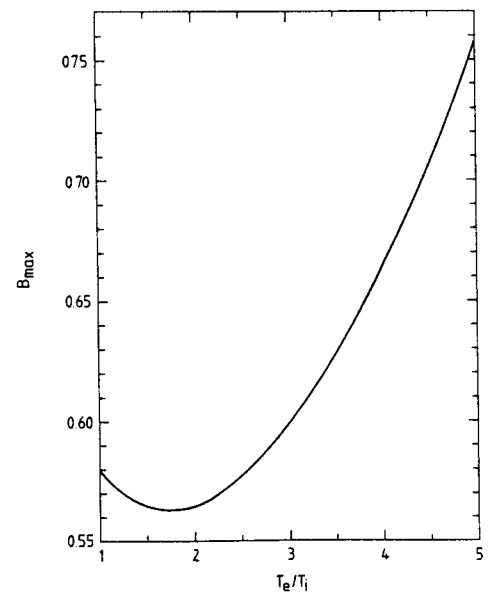


Fig. A1. Maximum of $B(\alpha, T_e/T_i)$, B_{\max} , as a function of T_e/T_i .

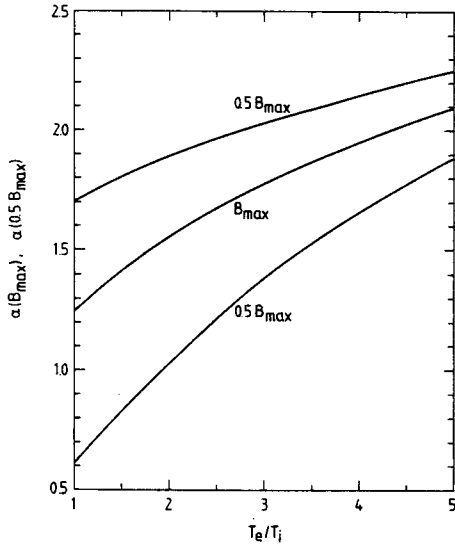


Fig. A2. $\alpha(B_{\max})$ and $\alpha(0.5 B_{\max})$ as a function of T_e/T_i .

almost exactly the reflection height z_0 , (A8a) is simplified to

$$k_{1D} = \sqrt{\frac{2}{3}} \frac{\omega_0}{V_e} \sqrt{\delta} \quad (\text{A9})$$

and k_{1D} is now entirely a function of altitude, upon specification of ω_0 and T_e . Equations (A7) and (A9) yield

$$\omega_{2D} = \omega_0 \sqrt{\frac{2}{3}} \alpha \frac{V_i}{V_e} \sqrt{\delta} \quad (\text{A10})$$

ω_{2D}/ω_0 versus δ , for O^+ ions and $\alpha = \alpha(B_{\max})$, is shown in Figure A3. The corresponding frequency spreads are given by

$$\Delta\omega_{2D}^{\pm} = \omega_0 \sqrt{\frac{2}{3}} \Delta\alpha^{\pm} \frac{V_i}{V_e} \sqrt{\delta} \quad (\text{A11})$$

with $\Delta\alpha^+$ taken as the difference between the upper and middle curve in Figure A2, and $\Delta\alpha^-$ the difference between the middle and lower curve in Figure A2.

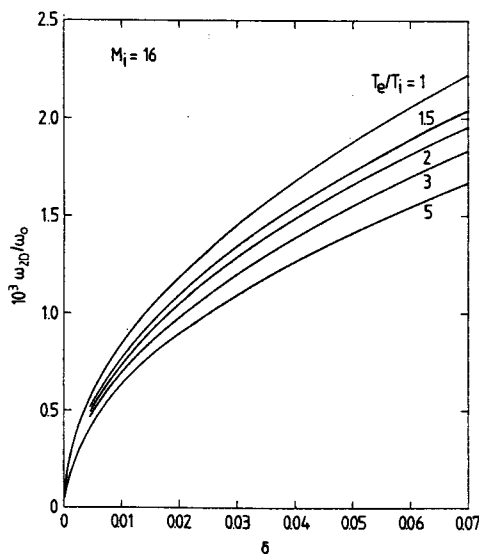


Fig. A3. ω_{2D}/ω_0 as a function of δ . The frequency of primary ion acoustic waves excited by the parametric decay instability is represented by ω_{2D} .

Another quantity that we need in section 3 is the wave number spread, which follows from (A8a) and (A8b) as

$$\Delta k_{1D} = \frac{1}{3} \Delta\alpha \frac{\omega_0 V_i}{V_e^2} \quad (\text{A12})$$

Next we consider the cascade products, LWC and IAC. It follows from (A2) and the properties of $B(\alpha)$ that the threshold of the secondary decay instability is lowest if the wave vectors of the mother and daughter Langmuir waves are antiparallel. Thus

$$\mathbf{k}_{1C} = (-1)^c \mathbf{k}_{1D} \quad (\text{A13})$$

where the integer c denotes the c th cascade product ($c = 1, 2, \dots$). Using (A13) in (A6) and comparing with (A7),

$$\omega_{2C} = 2\omega_{2D} \quad (\text{A14})$$

From (A14) and (A1),

$$\omega_{1C} = \omega_0 - (2c + 1)\omega_{2D} \quad (\text{A15})$$

APPENDIX B: STANDING WAVE PATTERN OF THE ELECTROMAGNETIC PUMP NEAR THE REFLECTION POINT

For a linear electron density profile, the electric field strength of the pump versus altitude is given by [see Budden, 1961, chapter 16]

$$E = E_0 \text{Ai}(-\zeta) \quad (\text{B1a})$$

$$\zeta \equiv (k_0^2/H)^{1/3} (z_0 - z) = 2(k_0 H)^{2/3} \delta \quad (\text{B1b})$$

with $k_0 = \omega_0/c$ the vacuum wave number, H the linear electron density scale height and δ as defined by (1). A useful approximation to the Airy function, valid for $\zeta \gtrsim 1.5$, is given by

$$\text{Ai}(-\zeta) = 0.564 \zeta^{-1/4} \sin\left(\frac{\pi}{4} + \frac{2}{3} \zeta^{3/2}\right) \quad (\text{B2})$$

The first Airy maximum, not described by (B2), is

$$\zeta_1 = 1.02 \quad \text{Ai}(-\zeta_1) = 0.536 \quad (\text{B3a})$$

The further extrema, as given by (B2), are ($m = 2, 3, \dots$)

$$\zeta_m = \left[\frac{3\pi}{4} \left(2m - \frac{3}{2} \right) \right]^{2/3} \quad (\text{B3b})$$

$$\text{Ai}(-\zeta_m) = (-1)^{m-1} 0.564 \zeta_m^{-1/4} \quad (\text{B3b})$$

The zeros occur at ($n = 1, 2, \dots$)

$$\zeta_n = \left[\frac{3\pi}{2} \left(n - \frac{1}{4} \right) \right]^{2/3} \quad (\text{B4})$$

An important quantity in our considerations is the swelling factor s within the height range in which the parametric decay instability can be excited. This height range is given by $0 \leq \delta \leq \delta_{\max} \approx 0.05$. We define the swelling factor s here as the ratio of E^2 at the Airy extrema to E^2 at the Airy extremum that lies closest to δ_{\max} . From (B1b), (B3a), and (B3b) we obtain

$$s(\zeta_m) = 0.29 \zeta_m^{-1/2} (k_0 H)^{1/3} \quad (m \geq 2) \quad (\text{B5})$$

$$s(\zeta_1) = 0.26 (k_0 H)^{1/3} \quad (m \geq 2)$$

A typical value of $s(\zeta_1)$, for $f_0 \equiv \omega_0/2\pi = 5$ MHz and $H = 50$ km, is 4.5 (or 6.5 dB).

APPENDIX C: FREQUENCY SPREADS OF LWC AND IAC WAVES

We change the notation slightly here in order to obtain a more concise formulation. In the following, E_{00} is the field strength of the EM pump, and E_c are the field strengths of the LWD wave ($c = 0$) and the LWC waves ($c = 1, 2, \dots$). Furthermore, we introduce the symbols $e_{00} \equiv (E_{00}/E_{0th})^2$ and $e_c \equiv (E_c/E_{0th})^2$. Our working assumption is that E_c is determined by energy gain from $c - 1$, by energy loss through collisions and Landau damping, and by energy loss through excitation of $c + 1$ [see *Kuo and Fejer, 1972*]. The energy balance of the LWD wave can then be written, with (A2), as

$$\frac{\omega_0 \epsilon_0^2 B}{8N_e K T_i} E_{00}^2 E_0^2 = \frac{\epsilon_0}{2} \nu E_0^2 + \frac{\omega_0 \epsilon_0^2 B}{8N_e K T_i} E_0^2 E_1^2 \quad (C1a)$$

At threshold

$$\frac{\omega_0 \epsilon_0^2 B}{8N_e K T_i} E_{0th}^2 = \frac{\epsilon_0}{2} \nu \quad (C1b)$$

and thus

$$e_{00} = 1 + e_1 \quad (C1c)$$

Corresponding expressions can be obtained for the other c 's, and we thereby obtain the following system of equations

$$\begin{aligned} e_{00} &= 1 + e_1 \\ e_0 &= 1 + e_2 \\ e_1 &= 1 + e_3 \\ &\vdots \\ e_{c-1} &= 1 + e_c \end{aligned} \quad (C2)$$

The solution for the e 's with odd indices follows as

$$e_{2j+1} = e_{00} - (j + 1) \quad (j = 0, 1, \dots) \quad (C3)$$

With $m \equiv \text{int}(e_{00})$ (i.e., m is the nearest smaller integer to e_{00}), the last positive e_{2j+1} is obtained for $j = m - 1$, and e_{2j+1} is thus given by

$$\begin{aligned} e_{2j+1} &= e_{00} - (j + 1) & j \leq m - 1 \\ e_{2j+1} &= 0 & j > m - 1 \end{aligned} \quad (C4)$$

e_{2m-1} is positive, but below threshold, and so $e_{2j} = 0$ for $j \geq m$. Thus, the e 's with even indices are given by

$$\begin{aligned} e_{2j} &= m - j & j < m \\ e_{2j} &= 0 & j \geq m \end{aligned} \quad (C5)$$

The major weakness in the above considerations is the tacitly made assumption that energy exchange between two waves only occurs at the maximum of B . Another significant, although not equally serious, restriction is the assumption that energy exchange takes place only between neighboring waves. It is a result of these assumptions that e_{2j} as a function of e_{00} shows discontinuities at $e_{00} = 1, 2, 3, \dots$ and is constant between two such discontinuities.

Once e_c is known, the frequency spread for $c + 1$ is obtained in the following way: We define

$$\alpha^\pm \equiv \alpha \left(\frac{1}{e_c} \cdot B_{\max} \right) \quad (C6a)$$

with α^+ the larger and α^- the smaller of these two values, and

$$\Delta\alpha^+ \equiv \alpha^+ - \alpha(B_{\max}) \quad (C6b)$$

$$\Delta\alpha^- \equiv \alpha(B_{\max}) - \alpha^- \quad (C6c)$$

With these definitions, we immediately obtain for the frequency spread of the IAC cascade product $c + 1$

$$\Delta\omega_{2c}^\pm(c + 1) = \frac{\Delta\alpha^\pm}{\alpha} \omega_{2c}(c + 1) \quad (C7a)$$

In this relation the mother wave enters only through its value of e_c , but not through its inherent frequency spread. Obviously,

$$\Delta\omega_{2c}^\pm(c + 1) \geq \Delta\omega_{2c}^\pm(c) \quad (C7b)$$

We can combine (C7a) and (C7b) into

$$\Delta\omega_{2c}^\pm(c + 1) = \text{Max} \left(\Delta\omega_{2c}^\pm(c), \frac{\Delta\alpha^\pm}{\alpha} \omega_{2c}(c + 1) \right) \quad (C8)$$

and furthermore have, as a consequence of the frequency selection rule,

$$\Delta\omega_{1c}^\pm(c + 1) = \Delta\omega_{2c}^\mp(c + 1) \quad (C9)$$

If we now assume $e_{00} = 2$ as in the evaluation of the frequency spreads given by (28b) and (28c), we have $e_1 = 1$ and $e_0 = 1$ or 2 , $e_2 = 0$ or 1 , depending on whether $e_{00} = 2 - \epsilon$ or $e_{00} = 2 + \epsilon$. In order to remove this ambiguity, we take $1 \leq e_0 \leq 2$; e_2 is not needed because $e_3 = 0$. From (C8) and (2e)

$$\Delta\omega_{2D}^\pm \leq \Delta\omega_{2C}^\pm \leq 2\Delta\omega_{2D}^\pm \quad c = 1 \quad (C10)$$

Acknowledgments. We wish to acknowledge the financial support given to the Heating project by the Deutsche Forschungsgemeinschaft (DFG). Thanks are due to the Auroral Observatory, Tromsø, for making available to us the field station at Lavangsdalen. One of the authors (B.T.) gratefully acknowledges financial support of the Swedish Science Research Council (NFR).

The Editor thanks P. Palmadesso and B. Cragin for their assistance in evaluating this paper.

REFERENCES

- Budden, K. G., *Radio Wave in the Ionosphere*, Cambridge University Press, New York, 1961.
- Fejer, J. A., Ionospheric modification and parametric instabilities, *Rev. Geophys. Space Phys.*, **17**, 135-153, 1979.
- Fejer, J. A., and E. Leer, Excitation of parametric instabilities by radio waves in the ionosphere, *Radio Sci.*, **7**, 481-491, 1972.
- Kohl, H., C. LaHoz, K. Folkestad, T. Hansen, H. Kopka, G. Rose, and P. Stubbe, The electron and ion spectra of radar returns from the critical height during ionospheric heating experiments, *Eur. Space Agency Spec. Publ.*, SP-195, 91-97, 1983.
- Kuo, Y. Y., and J. A. Fejer, Spectral-line structure of saturated parametric instabilities, *Phys. Rev. Lett.*, **29**, 1667-1670, 1972.
- Stubbe, P., H. Kopka, H. Lauche, M. T. Rietveld, A. Brekke, O. Holt, T. B. Jones, T. Robinson, A. Hedberg, B. Thidé, M. Crochet, and H. J. Lotz, Ionospheric modification experiments in northern Scandinavia, *J. Atmos. Terr. Phys.*, **44**, 1025-1041, 1982.
- Thidé, B., H. Kopka, and P. Stubbe, Observations of stimulated scattering of a strong high-frequency radio wave in the ionosphere, *Phys. Rev. Lett.*, **49**, 1561-1564, 1982.
- Thidé, B., H. Derblom, A. Hedberg, H. Kopka, and P. Stubbe, Observations of stimulated electromagnetic emissions in ionospheric heating experiments, *Radio Sci.*, **18**, 851-860, 1983.
- H. Derblom and B. Thidé, Uppsala Ionospheric Observatory, S-755 90 Uppsala, Sweden.
- H. Kopka and P. Stubbe, Max-Planck-Institut für Aeronomie, Postfach 20, D-3411 Katlenburg-Lindau 3, Federal Republic of Germany.

(Received January 13, 1984;
accepted April 25, 1984.)